Available online at www.sciencedirect.com
SCIENCE DIRECT®
Journal of Solid State Chemistry 177 (2004) 3553–3559
JOURNAL OF SOLID STATE CHEMISTRY
http://elsevier.com/locate/jssc

Synthesis of $PbTiO_3$ ceramics using mechanical alloying and solid state sintering

Jennifer S. Forrester,[a,*] Jennifer S. Zobec,[b] David Phelan,[b] and Erich H. Kisi[a]

[a] *School of Engineering, University of Newcastle, University Drive, Callaghan 2308, New South Wales, Australia*
[b] *Electron Microscope and X-ray Unit, University of Newcastle, Callaghan 2308, Australia*

Received 19 March 2004; received in revised form 28 May 2004; accepted 4 June 2004

Available online 11 August 2004

Abstract

The pressure-less sintering behavior of $PbTiO_3$ powders synthesized by mechanical alloying TiO_2 and PbO was investigated using dilatometry and Rietveld refinements of X-ray diffraction patterns. As-synthesized, the powders are nanocrystalline with a mean particle size of 20 nm. Pressure-less sintering in the range 500–1050°C gives single phase ceramics with densities of 85–90% and crystallite sizes in the range 80–400 nm. Cracking due to the paraelectric–ferroelectric phase transition was not observed in samples sintered below 700°C due to the small crystallite size whereas macroscopic cracks formed in samples sintered above 700°C. Rietveld analysis indicates the formation of Pb vacancies in samples sintered and held for 24 h at intermediate temperatures (600–1000°C) which gives some insight into the mechanism of Pb loss and second phase formation in this system.

Keywords: Lead titanate; $PbTiO_3$; Mechanical alloying; Rietveld analysis; Low-temperature sintering; Lead volatilization

1. Introduction

$PbTiO_3$ (PT) is used in a range of piezoelectric applications, as well as being the end-member of technologically significant ferroelectric perovskite series such as $PbZr_{(x)}Ti_{(1-x)}O_3$(PZT), $Pb_{(x)}Ca_{(1-x)}TiO_3$, $Pb(Zn_{1/3}Nb_{2/3})O_3-(x)PbTiO_3$(PZN-PT) and $Pb(Mg_{1/3}Nb_{2/3})O_3-(x)PbTiO_3$(PMN-PT). At ambient temperature, the material has a strong anisotropy which develops during cooling through the cubic-tetragonal phase transition of approximately 490°C. The anisotropy as measured by the tetragonality of the unit cell, c/a, may be as high as ~ 1.06 [1]. A large c/a ratio is considered favorable for enhanced electrical properties [2]. Unfortunately, pure $PbTiO_3$ has been difficult to synthesize as a mechanically robust, high density, monolithic ceramic. Problems typically encountered include Pb loss, porosity and microcracking, in extreme cases leading to spontaneous fracture.

The primary hurdle in PT fabrication is the synthesis of a single phase with the required perovskite structure. The difficulty is due to the volatility of PbO at elevated temperatures. The $PbTiO_3$ structure can only tolerate minor amounts of Pb-loss, higher levels of which effectively promote second phase formation and the degradation of piezoelectric properties. An example is the formation of a PT phase with the pyrochlore structure observed during a co-precipitation synthesis experiment [3]. A more common occurrence is the formation of a two-phase mixture with TiO_2 [4]. The volatilization of PbO is known to increase markedly at temperatures above 800°C, though the critical temperature is debated. Kim et al. [5] have stated that a PbO-rich PT will form a liquid phase above 838°C, Algueró et al. [6] found that at 650°C an excess of 20% PbO was required because of Pb-loss during thermal treatments of sol–gel prepared La-modified PT thin films, whereas Ananta and Thomas [7] found Pb volatility in PMN-PT could be minimised by careful sintering up to 1250°C. What is clear is that the losses depend on particle size, processing conditions and chemical stability. The degree of Pb incorporation into the pre-sintered crystal

*Corresponding author. Fax: +61-2-4921-7050.
E-mail address: jforrest@mail.newcastle.edu.au (J.S. Forrester).

0022-4596/$ - see front matter © 2004 Elsevier Inc. All rights reserved.
doi:10.1016/j.jssc.2004.06.005

structure affects the volatility enormously [4]. Many groups report that Pb-loss may be minimised by sintering compacted powders in a surrounding Pb-based powder or a PbO vapor atmosphere [5,8] although this may lead to a Pb gradient in the final sintered product [4].

The problem of porosity has largely been addressed through particle size control of the starting powder. A fine powder with minimal particle agglomeration is suitable as the precursor to a dense fired ceramic. To achieve this various chemically based approaches have been used; for example sol–gel synthesis has been able to produce dense ceramics with a crystallite size of approximately 20 nm, by sintering at temperatures as low as 400°C [9]. Other methods for production of PT ceramics include spark-plasma-sintering of hydrothermally prepared PT powders at >900°C for 1–3 min [10]. The high temperature combined with a short sintering time can result in small grain sizes (<1 μm). Co-precipitation [11], emulsion techniques [12] and solvothermal synthesis [13] are other methods employed to produce fine powders.

Microcracking in monolithic $PbTiO_3$ ceramics has also been addressed by particle size control. Tartaj et al. [9] using sol–gel preparation found grain sizes of 0.5–1 μm following sintering at 1100°C for 2 h. Samples hot-pressed at 800°C by Matsuo and Sasaki [14] were uncracked when the grain size was less than 1 μm. Using co-precipitation, Archer et al. [3] achieved crystallite sizes of ~30 nm, and similarly the co-precipitation of Duran et al. [15] led to sintered compacts without microcracking provided the grain size was less than 1 μm. It is clear from these investigations that it is commonly believed that a fine grain size in PT is essential for high density and little or no microcracking.

Mechanical alloying (MA) can provide an alternative means of minimizing the problems of cracking, porosity and Pb volatility. It has been shown that homogeneous powders with a fine grain size can be created by the MA process. For example, Xue et al. [16] found that following 10 h of milling, the particle sizes of PT were 20–30 nm. Careful sintering at lower than normally employed temperatures may restrict grain growth, and on cooling internal strains are reduced avoiding cracking. In addition, because these nano-particles may be sintered at lower temperatures, the problem of Pb volatility is minimized.

MA has been successful in the alloying of metals, and recently the alloying of oxides has gained prominence. Several perovskite structures have been produced (PZT produced by Branković et al. [17]; $0.9Pb[(Zn_{0.6}Mg_{0.4})_{1/3}Nb_{2/3}O_3]-0.1PbTiO_3$ produced by Wan et al. [18]). However, possibly due to the small grain sizes and high strains developed during MA, it has often been difficult to retain the desired phases when the powders are sintered [19].

Xue et al. [16] have published a procedure for producing PT powders directly from the constituent oxides (PbO and TiO_2) by mechanically alloying. There was however no subsequent analysis of the sintering behavior of the powders. In this paper, we have adopted the powder production procedure of Xue et al. and investigated the sintering behavior of the powders at various temperatures using dilatometry. The sintered compacts were analyzed using Rietveld refinement of X-ray diffraction (XRD) patterns and scanning electron microscopy.

2. Experimental section

The reactant powders were commercially available PbO (>99% purity, BDH Chemicals, Australia) and TiO_2 (anatase form, >99% purity, Johnson Matthey, Germany). Stoichiometric quantities were weighed to form PT, and these were placed in a pre-conditioned zirconia vial with yttria tetragonal zirconia grinding balls (10 mm in diameter). The ball:powder ratio was 20:1. Dry milling was conducted in a SPEX 8000 mixer-mill. XRD showed that PT phase formation was complete after 24 h of milling. XRD patterns were collected from powders after the completion of milling for phase identification, and to be used for later Rietveld analyses. These were collected using a Philips 1710 powder diffractometer with Cu$K\alpha$ radiation in the range 10–90° 2θ with a 0.04° step size. The collection times varied according to sample perfection.

Milled powders for the sintering experiments were loaded into a die and uniaxially pressing at approximately 100 MPa. Samples were placed in an alumina crucible in a bed of PbO and covered by an alumina lid, sintered for 24 h in air at 500, 600, 700, 800, 900, 1000 and 1050°C, followed by air cooling. The long sintering times were chosen because it was important to ascertain the phase stability of the perovskite PT structure.

For dilatometer tests, 8 g of milled powder was uniaxially pressed in a 12 mm die and sintered in an in-house constructed dilatometer. Two modes of operation were adopted. In the first constant heating mode, samples were heated at 5°C/min to the selected maximum temperature, held for 10 min and returned to room temperature at 10°C/min. In the second, samples were heated at 5°C/min and held at constant temperature for 14 h.

The surfaces of the pellets were removed prior to XRD pattern collection by gently grinding with 400-grit SiC emery paper so that excess surface PbO was removed. Rietveld refinement was performed using the computer program LHPM [20]. The crystallographic data for the refinement were initially those of Glazer and Mabud [21]. The global parameters refined were the zero point, scale factor and four coefficients of a background

polynomial. Additional structural and instrumental parameters were refined as follows:

(i) The lattice parameters (a and c).
(ii) The full-width of the Lorentzian component of the Voigt peak shape function (k) so that the crystallite size could be examined.
(iii) The March coefficient, r, which is useful in modeling preferred orientation.
(iv) The Gaussian half-width parameter, U, as it is associated with internal strains in a sample.
(v) The occupancy of the Pb site of the crystal structure.

The instrumental variables, i.e., the asymmetry parameter and the peak width parameters V and W were fixed at 0.005, −0.0027 and 0.0036, respectively, following the refinement of a NIST standard.

Samples were examined using a Philips XL30 scanning electron microscope (SEM), operated at 15 kV. The microscope is fitted with an Oxford ISIS Si/(Li) energy dispersive spectroscopy (EDS) detector. Secondary electron images were obtained from the as-milled powder and from the sintered compacts. Both the as-sintered surfaces and fracture surfaces were examined.

3. Results

The physical condition of the sintered ceramics varied as a function of temperature. Samples sintered at 500°C, 600°C, 700°C and 800°C were monolithic and relatively robust. Those sintered at greater temperatures showed greater degrees of cracking until at 900°C, the sample spontaneously fractured.

X-ray diffraction patterns collected from a mechanically alloyed powder and samples sintered at 500°C, 700°C and 900°C and 1050°C are shown in Fig. 1. At the resolution available, there are no indications of unreacted starting powders after milling. The powder diffraction peaks from PT produced by milling are considerably broadened (Fig. 1a). In addition, considerable asymmetry of the diffraction peak at $\sim 31°$ 2θ is apparent. This asymmetry has been widely visible following the milling of similar powders [17,18], although it has not been previously noted nor has its origin been identified. XRD patterns of sintered samples show that the asymmetry is easily eliminated by sintering. Following sintering at 500°C, the diffraction peaks have narrowed substantially, and the PT phase has persisted without evidence of second phase formation. Sintering at higher temperatures does not appear to substantially alter the patterns. However, the XRD patterns collected at the highest temperatures (Figs. 1d and e) do show very minor diffraction peaks, suggestive of second phase development (indicated by arrows).

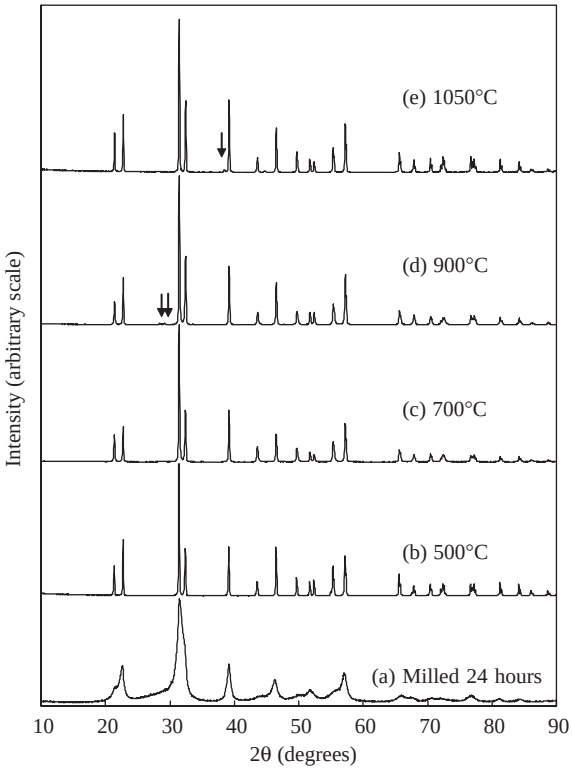

Fig. 1. (a–e) XRD patterns of milled PT and compacts sintered at selected temperatures.

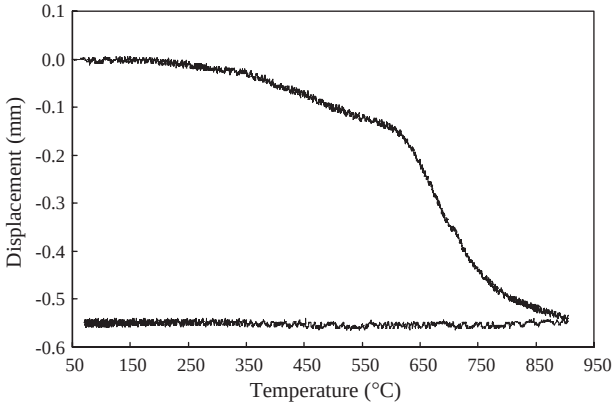

Fig. 2. Dilatometer test of $PbTiO_3$ green compact during heating from 50°C to 900°C, with data collected with decreasing temperature.

Examples of dilatometer results are shown in Figs. 2 and 3. The results shown in Fig. 2 are for a sample heated to 900°C, held for 10 min and then cooled. There is little change in the sample to approximately 350°C. Some pre-sintering densification occurred between 350°C and approximately 630°C. The significant slope change above 630°C indicates a marked increase in the sample densification rate and the onset of true sintering. At about 800°C the slope decreases, indicating that the majority of densification has occurred below this temperature. To extend this notion, a compact was

heated to 700°C and held there for 14 h. The displacement versus time data is shown in Fig. 3. The same slope changes in Fig. 2 are evident in Fig. 3. The decrease in slope and levelling after 4–5 h indicates that sintering is mostly complete after 14 h at 700°C.

Results of the Rietveld analyses of XRD patterns from the milled powder and samples sintered at various temperatures are presented in Tables 1 and 2, and the refinement of the XRD pattern of a sample sintered at 700°C is shown in Fig. 4. The refined parameter values given are for refinements that include refinement of the Pb occupancy, apart from the as-milled sample where the breadth of the diffraction peaks made its refinement difficult. The rms agreement between the calculated and observed integrated intensities, R_B, prior to and following Pb occupancy refinements are given in Table 1 for comparison.

Some interesting trends were revealed:

1. The unit cell dimensions are not significantly influenced by the sintering temperature. The c/a ratio increases from 1.04 to 1.06 upon sintering at 500°C, but does not vary significantly with sintering temperature thereafter.
2. The refined occupancy of the Pb position is highest in the as-milled sample and that sintered at the highest temperature, and is considerably less for intermediate temperatures.
3. The refined Gaussian half-width parameters (U) are all small suggesting that inter-particle strains may contribute little to the diffraction peak shapes in these samples.

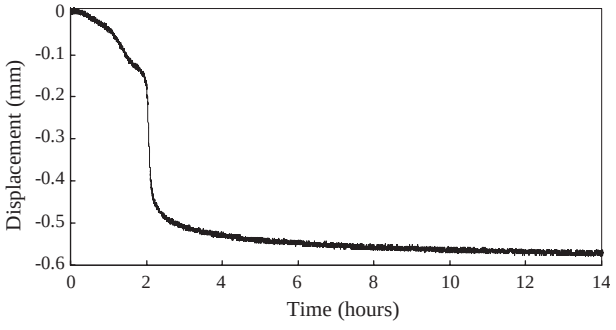

Fig. 3. Dilatometer test of $PbTiO_3$ held at 700°C for 14 h.

Table 2
Refined U, Lorentzian FWHM, and March coefficient

Sintering temperature	Gaussian FWHM (U)	Lorentzian FWHM	March coefficient (r)
Not sintered	0.56(2)	0.79(2)	1.086(9)
500°C	0.017(2)	0.139(4)	1.010(8)
600°C	0.031(1)	0.117(8)	1.028(4)
700°C	0.036(3)	0.088(1)	0.943(7)
800°C	0.030(2)	0.081(2)	0.976(7)
900°C	0.048(3)	0.072(1)	1.032(7)
1000°C	0.109(6)	0.061(2)	1.020(5)
1050°C	0.136(2)	0.054(1)	0.995(8)

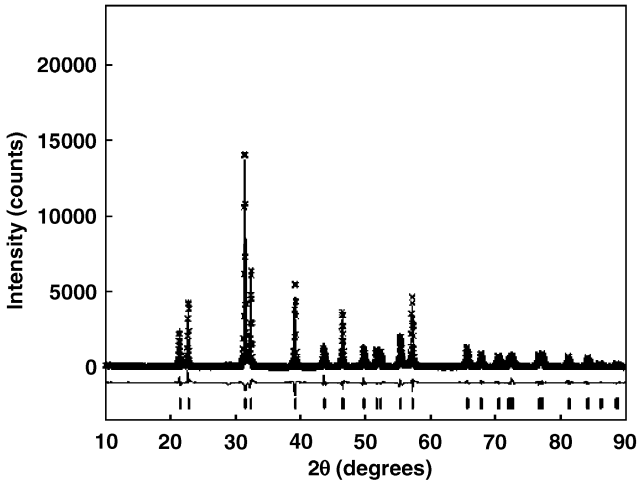

Fig. 4. Rietveld analysis of $PbTiO_3$ milled for 24 h and sintered at 700°C for 24 h. The crosses represent the experimental pattern, the line is the calculated pattern, and the line below is the difference pattern between the calculated and experimental data. Below this are the $h\,k\,l$ markers for the PT structure.

Table 1
Refined lattice parameters, c/a ratio, Pb occupancy, and R_B factors before and after Pb occupancy is refined

Sintering temperature	a (Å)	c (Å)	c/a Ratio	Refined Pb occupancy	R_B (Pb occupancy not refined)	R_B (Pb occupancy refined)
Not sintered	3.914(1)[a]	4.094(2)	1.046	—	2.71	—
500°C	3.9018(1)	4.1503(1)	1.0637	1.025(3)	8.08	7.71
600°C	3.9021(2)	4.1404(3)	1.0611	0.943(4)	4.71	3.97
700°C	3.9004(1)	4.1472(1)	1.0633	0.914(3)	5.09	3.48
800°C	3.9024(1)	4.1486(1)	1.0631	0.880(3)	5.21	3.29
900°C	3.9016(1)	4.1467(2)	1.0628	0.887(3)	5.07	3.30
1000°C	3.9032(1)	4.1430(3)	1.0615	0.877(4)	7.17	5.82
1050°C	3.9025(1)	4.1509(2)	1.0637	0.993(3)	4.77	4.78

[a] The number in parentheses refers to the right-hand digit and represents the standard deviation estimated in the Rietveld analyses.

4. There is little noticeable trend in the preferred orientation as shown by the values of the March coefficient in Table 2.
5. The parameter representing the width of the Lorentzian component of the peaks (k), decreases with increased sintering temperature. This is indicative of grain growth at the higher temperatures and has been quantified using the Scherrer equation leading to the particle sizes calculated from Table 2. The particle size following milling is approximately 20 nm. Sintering at higher temperatures increased the particle size from approximately 170 nm at 500°C to around 400 nm at 1050°C. These are average values and do not reflect the distribution of particle sizes within the compact.

SEM micrographs of the fracture surfaces of compacts sintered at 700°C and 900°C are shown in Figs. 5a and b, respectively. Fig. 4a shows that the sample has developed a relatively uniform microstructure with a grain size of 200–400 nm. Some residual porosity is visible and the fracture appears to have been intergranular. Sintering at 900°C leads to a superficially similar microstructure except that some abnormal grain growth occurs. For example, a large grain is visible in Fig. 5b (around 1.5–2 μm in diameter) surrounded by smaller particles. Overall, at 900°C, the particle size distribution is much broader. There are areas of the fracture surface with a regular arrangement of small grains, whereas in other areas grains as large as 6 μm have grown. It is likely that the growth of large grains locally increases internal stresses and leads to cracking in the bulk ceramic on cooling.

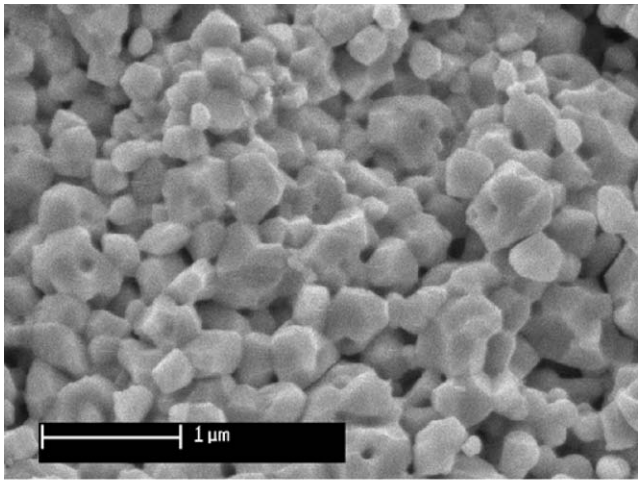

(a)

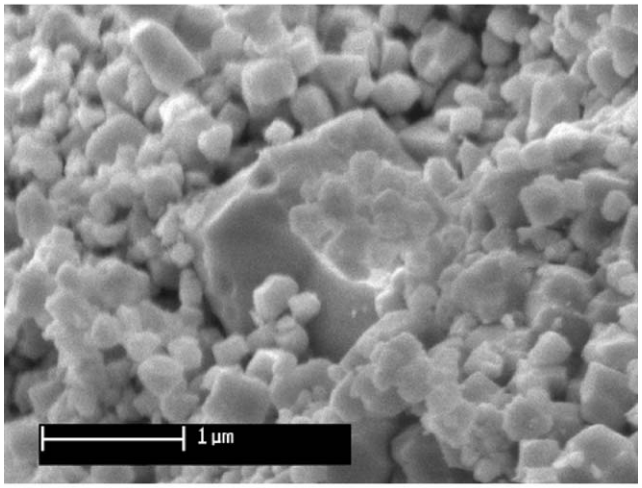

(b)

Fig. 5. SEM micrographs of fracture surfaces of $PbTiO_3$ samples sintered (a) at 700°C and (b) at 900°C.

4. Discussion

4.1. Synthesis

The first outcome of these experiments is to confirm that $PbTiO_3$ (PT) can be relatively simply synthesized by mechanically alloying stoichiometric mixtures of PbO and TiO_2 as indicated in the work of Xue et al. [16]. The as-milled PT appears to be crystalline, with an extremely fine crystallite size. Within the sensitivity of the highly broadened X-ray diffraction peaks, no extraneous phases were observed.

The second outcome is that the PT formed by mechanical alloying is stable (i.e., no additional phases visible) during sintering for 24 h in air (with a PbO shroud) at temperatures up to 800°C. Stability is still very good (i.e., only minimal second phase formation) during sintering for 24 h at temperatures up to 1050°C in air.

4.2. Sinterability

The third outcome is that the milled powders are readily sintered. Sintering trials indicate that minor (pre-sintering) densification occurs at temperatures as low as 350°C (Fig. 2), however samples sintered at 400°C had no inter-particle bond strength and were extremely friable upon removal from the furnace. True sintering did however occur within 24 h at temperatures as low as 500°C. This is in agreement with literature reports of very low sintering temperatures for sol–gel prepared powders (e.g., 400°C, [9]) and is believed to be due to the very fine crystallite size of the milled powder (20 nm). The rate of sintering is quite high, for example the bulk of the densification occurs within 15 min of the sample reaching 700°C in Fig 2. The final sintered densities are only moderate (generally between 85% and 90% of theoretical density) as no special precautions were taken

to de-agglomerate the milled powders prior to pressing and no pressure was applied during sintering.

4.3. Microcracking

Using the Rietveld refined unit cell data, the *c*/*a* ratio in milled PT was calculated as 1.0467. Sintering anywhere in the temperature range 500–1050°C is associated with an increase in the c/a ratio to 1.0625 ± 0.0010. It has been stated in the literature [15] that there is a critical c/a ratio above which microcracking will occur. In La-modified PT this ratio is ~ 1.05, and in Ca-modified PT this ratio is ~ 1.04. In un-doped PT, the c/a ratio is typically 1.06 and hence, based upon the above criterion, is susceptible to microcracking. For example, Kim et al. [5] found that sintered compacts with different grain sizes caused by a deficiency, excess or stoichiometric quantity of PbO in the initial composition all resulted in similar c/a ratios of approximately 1.06. Similarly, Takeuchi et al. [10] sintered samples from 900°C to 1200°C and found that the c/a ratio was 1.065 throughout. Those with the smallest grain sizes produced sintered compacts with the highest density and least microcracking.

There is considerable additional support in the literature to the notion that grain size is a critical influence in cracking and porosity in PT bulk ceramics [5,11]. PT samples with an average grain size of 1.8 μm formed dense ceramics, while samples with average grain sizes of 14.3 μm cracked during sintering. It was suggested that this is due to lower residual stress over small grains. In the work presented here, the grain size is around 0.02 μm following milling in agreement with the work of Xue et al. [16]. X-ray diffraction patterns recorded from samples sintered at 500°C (Fig. 1, Table 1) show that considerable grain growth had occurred. The trend of increasing *average* grain size as a function of sintering temperature is shown in Fig. 6 to be approximately exponential as expected. However, even at the highest temperature, the material appears to be relatively grain growth resistant, maintaining an average grain size below 0.5 μm even after 24 h at 1050°C. Similar results have been observed for sol–gel prepared powders [9], where grain sizes were only 0.5–1 μm following sintering at 1100°C for 2 h. The physical condition of the sintered ceramics considered here are consistent with the view that, in systems prone to microcracking due to a large c/a ratio, grain size reduction is an effective method of reducing or eliminating microcracking.

4.4. Diffraction peak asymmetry

The asymmetry seen in the XRD peaks of the milled powder following MA appears to affect all peaks to a greater or lesser degree. Although it is not yet clear what causes the asymmetry, it could originate from several areas. For example, MA is known to produce amorphous materials in many cases, and the asymmetry could be due to such an amorphous contribution. Alternatively, it could arise from stacking faults (although this is normally shown by asymmetric peak shapes on the high 2θ side), or an asymmetric distribution of particle sizes, or a distribution in composition. The latter would have to allow for lattice expansion, i.e., Pb on the Ti site.

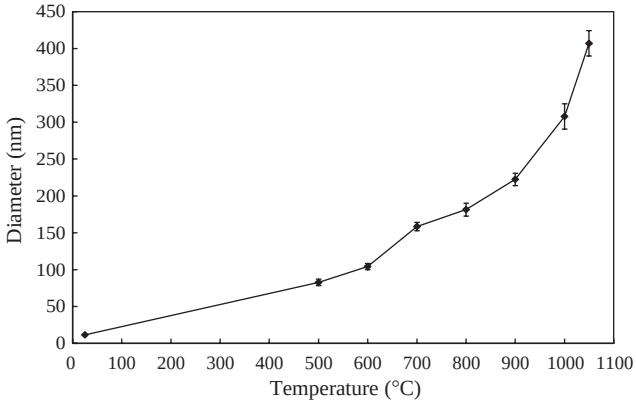

Fig. 6. Crystallite size as a function of temperature determined from X-ray diffraction line broadening. Error bars are plotted at one combined standard deviation of the observed Lorentzian half-width parameter k_{obs} and the instrumental Lorentzian half-width parameter k_i.

4.5. Pb occupancy

The refined occupancies shown in Table 1 indicate decreased Pb content for samples sintered at all but the lowest and highest temperatures. It is important that this apparent trend is interpreted with care. The estimated standard deviations from the Rietveld refinement (shown in parenthesis for the last digit) indicate that the deviations from stoichiometry are much larger than three standard deviations. As these standard deviations are estimated from random counting errors, there is still a residual possibility that the non-stoichiometry is due to undetected parameter correlations. It is unlikely that the entire effect is due to this cause, however the absolute uncertainty in the Pb occupancy is most likely underestimated by the standard deviations quoted in Table 1.

Notwithstanding the cautionary note above, the results do indicate significant lead loss and may be indicative of the Pb-loss mechanism. It would appear that the structure can tolerate Pb vacancies prior to the precipitation of second phases. The pattern of Pb loss is then the result of two competing mechanisms: the *loss* of Pb by volatilization and the *fixing* of Pb within the crystal structure by crystal growth. We presume in what follows that the Pb loss increases with increasing

temperature (cet par) but that it decreases with increasing crystallite size (based upon increased diffusion distance and reduced surface area). At 500°C, although the rate of crystal growth is very low, the rate of Pb volatilization is too low for any decrease to be observed over the 24 h of the sintering treatment. At temperatures in the range 600–1000°C, the Pb volatilization seems to occur before substantial crystal growth, leading to Pb deficiency. At the highest temperature, 1050°C, the crystal growth rate is so rapid that the Pb is trapped within the crystallites even after holding at this temperature for 24 h.

From this mechanism, the two strategies for avoiding Pb loss discussed widely in the literature (i) using nanocrystalline starting powders to enable sintering at low temperature (500°C in this case) or (ii) rapid heating and very short sintering treatments at very high temperatures (>1050°C in this case) appear to be reconciled. Further crystallographic studies using neutron diffraction during isothermal sintering treatments at the intermediate temperatures are being conducted to further investigate this point.

5. Conclusions

1. $PbTiO_3$ (PT) powders can be synthesized directly from the constituent oxides using conventional mechanical alloying.
2. According to dilatometry results, the onset of rapid sintering in mechanically alloyed PT powders is 630°C. Longer treatments (24 h) caused sintering as low as 500°C.
3. Sintering at or below 700°C results in a monolithic ceramic whereas sintering above 800°C leads to cracking, and spontaneous fracture at 1050°C.
4. There is a strong correlation between the crystallite size and the sintering temperature lending support to the notion that crystallite size determines the propensity for microcracking.
5. The c/a ratio does not differ between samples sintered at different temperatures and hence does not appear to be critical in influencing microcracking.
6. Changes in the crystallite size and the occurrence of Pb vacancies during sintering of mechanically alloyed PT powders between 500°C and 1050°C may be used to account for the Pb loss characteristics of PT and related ceramics.

Acknowledgments

The Australian Research Council is thanked for financial support.

References

[1] G. Shirane, S. Hoshino, J. Phys. Soc. Japan 6 (1951) 265–270.
[2] Y. Xu, Ferroelectric Materials and Their Applications, North-Holland, Amsterdam, 1991.
[3] L.B. Archer, C.D. Chandler, R. Kingsborough, M.J. Hampden-Smith, J. Mater. Chem. 5 (1995) 151–158.
[4] L.S. Hong, C.C. Wei, Mater. Lett. 46 (2000) 149–153.
[5] S. Kim, M. Jun, S. Hwang, J. Am. Ceram. Soc. 82 (1999) 289–296.
[6] M. Algueró, G. Drazic, M. Kosec, M.L. Calzada, L. Pardo, Bol. Soc. Esp. Ceram. Vidrio 41 (1999) 98–101.
[7] S. Ananta, N.W. Thomas, J. Eur. Ceram. Soc. 19 (1999) 2917–2930.
[8] K. Katayama, M. Abe, T. Akiba, H. Yanagida, J. Eur. Ceram. Soc. 5 (1989) 183–191.
[9] J. Tartaj, C. Moure, L. Lascano, P. Durán, Mater. Res. Bull. 36 (2001) 2301–2310.
[10] T. Takeuchi, M. Tabuchi, I. Kondoh, N. Tamari, H. Kakegama, J. Am. Ceram. Soc. 83 (2000) 541–544.
[11] S.R. Dhage, Y.B. Khollam, H.S. Potdar, S.B. Deshpande, B.D. Sarwade, D.K. Date, Mater. Lett. 56 (2002) 564–570.
[12] M.M. Wu, G.G. Wang, H.F. Xu, J.B. Long, F.L.Y. Shek, S.M.F. Lo, I.D. Williams, S.H. Feng, R.R. Xu, Langmuir 19 (2003) 1362–1367.
[13] D.R. Chen, R.R. Xu, J. Mater. Chem. 8 (1998) 965–968.
[14] Y. Matsuo, H. Sasaki, J. Amer. Ceram. Soc. 49 (1966) 229–230.
[15] P. Duran, J.F. Fdez Lozano, F. Capel, C. Moure, J. Mater. Sci. 23 (1988) 4463–4469.
[16] J. Xue, D. Wan, J. Wang, Mater. Lett. 39 (1999) 364–369.
[17] Z. Branković, G. Branković, C. Jovalekić, Y. Maniette, M. Cilense, J.A. Varela, Mater. Sci. Eng. A 345 (2003) 243–248.
[18] D.M. Wan, J.M. Xue, J. Wang, Acta Metall. 47 (1999) 2283–2291.
[19] M. Algueró, C. Alemany, B. Jiménez, J. Holc, M. Kosec, L. Pardo, J. Eur. Ceram. Soc. 24 (2004) 937–940.
[20] C.J. Howard, B.A. Hunter, Acomputer program for Rietveld analysis of X-ray and neutron diffraction patterns, ANSTO Lucas Heights Research Laboratories, 1997.
[21] A.M. Glazer, S.A. Mabud, Acta Crystallogr. B 34 (1978) 1065–1078.